PIER C

(Received 10 July 2025, Accepted 11 August 2025, Scheduled 21 August 2025)

Modal Analysis of Underground Cables in Stratified Frequency-Dependent Soils Using a Derivative-Free Iterative Method

Yahia Serbouti and Abderrahman Maaouni*

Research Laboratory in Computer Science and Telecommunications, Physics Department, LRIT, Faculty of Sciences, Mohammed V University, P. O. B. 104, Rabat, Morocco

ABSTRACT: This paper examines the impact of soil stratification and the frequency dependence (FD) of the Earth's electrical parameters on the transient response of underground cable systems, accounting for both earth-return admittance and impedance. A derivative-free iterative approach is proposed to overcome issues related to discontinuous modal transformation matrices that occur at certain frequencies when using conventional diagonalization algorithms. This method ensures smooth and continuous eigenvector tracking. Transient voltages and currents along cables are computed using a modal-domain-based transmission line model combined with Numerical Inverse Laplace Transform (NILT). Simulation results validate the proposed method's accuracy and stability, and highlight the significant influence of the stratified frequency-dependent (SFD) ground under various operating conditions. Finally, a reduced equivalent model of the three-phase underground system is established to facilitate further analysis.

1. INTRODUCTION

Accurate modeling of overhead lines and underground cables (OHLUGC) is essential for assessing the transient response of power networks. A multi-phase system (MPS) is characterized by distributed, frequency-dependent FD parameters where voltages and currents behave as propagating waves. To compute transient responses in such systems, the ground-return impedance and admittance for lossy soil must be carefully evaluated. In this context, initial formulations for the ground-return impedance of underground cables were proposed by Pollaczek [1], neglecting displacement currents and associated admittance. They were later extended by Sunde [2], who incorporated the effects of ground displacement currents. Since then, various generalized expressions for admittance and impedance have been derived for both single-phase [3–6] and multi-phase [7, 8] systems. These classical models assume a semi-infinite, homogeneous earth.

Further studies [9–14] have investigated the influence of frequency-dependent soil properties on the wave propagation and transient behavior in OHLUGC systems. In recent years, several methods have been proposed for measuring and modeling FD soil parameters [15–17]. Soil is characterized by its frequency-dependent conductivity $\sigma(f)$, relative permittivity $\epsilon_r(f)$, and the constant magnetic permeability μ which is assumed to be equal to the vacuum permeability μ_0. These soil parameters also depend on soil characteristics such as temperature, humidity, and soil particle size. To evaluate the effect of the FD soil parameters on the transient response of the MPS, the usual procedure used in the aforementioned works consists of calculating the ground-return impedance and admittance using a specific set of FD ground models. This is justified by the fact that the parameter $\sigma(f) + j\omega\epsilon_r(f)\epsilon_0$ appears directly in frequency-domain Maxwell equations.

In this context, Li et al. [9] evaluated the behavior of overhead transmission line parameters considering the frequency characteristics of soil parameters. The ground-return impedance of the line was evaluated with complex penetration depth. The conductivity and permittivity of the soil were measured using a broad band dielectric spectrometer accounting for the soil moisture content and temperature. De Conti and Emidio [10] adapted Marti's transmission line model [18] to consider the influence of FD soil parameters by substituting Carson's integrals [19] of limited validity, particularly for high-frequency in poorly conducting soils, by those of Nakagawa and Iwamoto [20]. Causal expressions proposed by Alipio and Visacro [16] to represent the FD behavior of $\sigma(f)$ and $\epsilon_r(f)$ have been adopted. Later, Papadopoulos et al. [21] investigated the impact of the soil's FD electrical properties on propagation characteristics of underground cables. Earth-return impedance and admittance proposed in [22] were used. Recently, Xue et al. [14] developed an extended transmission line approach involving a generalized earth-return impedance and admittance for underground cables based on complete solutions of Maxwell's equations [8].

To solve transmission-line equations in these settings, modal decomposition techniques [23, 24] are commonly employed to decouple multi-phase systems. This allows for independent treatment of each mode, while preserving the influence of FD behavior in the modal transformation matrices. However, in

* Corresponding author: Abderrahman Maaouni (maaouni.fsr@gmail.com).

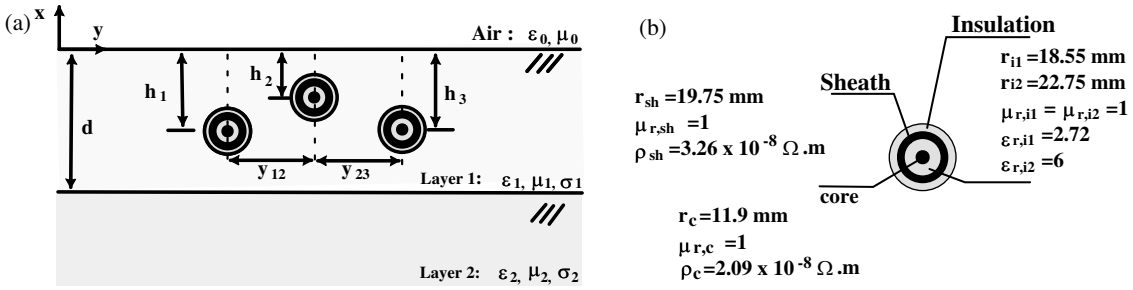

Geometric configuration of underground SC cables

Underground cable cross-section and data

FIGURE 1. Geometric configuration in two-layer earth.

complex cable configurations, standard eigenvalue solvers may fail to produce consistently ordered eigenvectors. As frequency varies, it often leads to unavoidable discontinuities or switching of modes. To achieve continuous and smooth eigenvectors and eigenvalues of **ZY** for power cables and lines, various iterative methods, including the modified Jacobi [25], Newton-Raphson [26], and Levenberg-Marquardt [27] methods were developed. For these methods, **ZY** is scaled as proposed in [28] to overcome overflow errors, and the eigenproblem is reformulated into an explicitly real-valued formulation.

This paper investigates the influence of stratification and frequency-dependent soil properties on the transient response of an underground cable system. The generalized quasi-transverse electromagnetic (TEM) earth-return impedance and shunt admittance model from [22] is adopted, along with the curve-fitting expressions of Longmire and Smith [15] for $\sigma(f)$ and $\epsilon_r(f)$. To ensure consistent modal tracking over frequency, we apply a derivative-free iterative scheme introduced in [29], enabling robust sorting and smoothing of modal quantities. Finally, a reduced model of a three-phase underground system is established.

2. SYSTEM UNDER STUDY

The geometric configuration of three single-core (SC) underground cables placed in a stratified earth medium is illustrated in Figure 1.

The soil consists of two layers. The cables are buried in the first layer at depths h_1, h_2, and h_3 from the air-soil interface, with horizontal spacings y_{12}, y_{23}, and $y_{13} = y_{12} + y_{23}$. The electrical properties of each layer are frequency dependent. The first layer has thickness d and is characterized by conductivity $\sigma_1(f)$ and permittivity $\varepsilon_1(f) = \varepsilon_0\varepsilon_{r1}(f)$. The second layer, extending to infinity in depth, is defined by $\sigma_2(f)$ and $\varepsilon_2(f) = \varepsilon_0\varepsilon_{r2}(f)$. Both layers are assumed to share the same permeability μ_0, with ε_0 and μ_0 denoting the vacuum permittivity and permeability, respectively.

Assuming quasi-transverse electromagnetic (TEM) propagation, the voltage and current wave propagation in the frequency domain is governed by the telegrapher's equations:

$$\frac{\partial \mathbf{V}}{\partial z} = -\mathbf{Z}(\omega)\,\mathbf{I}, \tag{1a}$$

$$\frac{\partial \mathbf{I}}{\partial z} = -\mathbf{Y}(\omega)\,\mathbf{V}, \tag{1b}$$

where ω is the angular frequency, and $\mathbf{V}$ and $\mathbf{I}$ are 6×1 vectors of phase voltages and currents, respectively. The 6×6 matrices $\mathbf{Z}(\omega)$ and $\mathbf{Y}(\omega)$ denote the per-unit-length series impedance and shunt admittance matrices, respectively. These matrices consist of the following components:

$$\mathbf{Z} = \mathbf{U} \otimes \mathbf{Z}_i + \mathbf{Z}_e \otimes \mathbf{J} \tag{2}$$

The operator $\otimes$ denotes the Kronecker (tensor) product, and the 3×3 matrices $\mathbf{U}$ and $\mathbf{J}$ are the unit and all-ones matrices, respectively. In Figure 1(b), the single-core cable is shown as a two-conductor system consisting of a core and a sheath, and the impedances are represented by a 2×2 matrix:

$$\mathbf{Z}_i = \begin{bmatrix} Z_{cci} & Z_{csi} \\ Z_{csi} & Z_{ssi} \end{bmatrix} \tag{3}$$

where Z_{cci} is the core self-impedance, Z_{ssi} the sheath self-impedance, and Z_{csi} the conductor-sheath mutual impedance. Expressions for the elements of impedance matrix $\mathbf{Z}_i$ based on the loop impedance formulation are given in [23].

The 3×3 matrix $\mathbf{Z}_e$ accounts for the earth-return path impedance of cables buried in the first layer in the two-layer soil model. According to Papadopoulos et al. [22], its elements are computed as:

$$Z_{e,ij} = \frac{j\mu_0}{2\pi} \int_0^\infty F(\lambda)\cos(y_{ij}\lambda)\,d\lambda, \tag{4}$$

with the kernel function $F(\lambda)$ defined as:

$$\begin{aligned} F(\lambda) = {} & \frac{1}{\alpha_1(s_{10}s_{21} - d_{10}d_{21}e^{-2\alpha_1 d})} \\ & \cdot \Big[s_{10}s_{21} - e^{-\alpha_1|h_i - h_j|} + s_{10}d_{21}e^{-\alpha_1(2d - h_i - h_j)} \\ & + d_{10}s_{21}e^{-\alpha_1(h_i + h_j)} + d_{10}d_{21}e^{-\alpha_1(2d - |h_i - h_j|)} \Big] \end{aligned} \tag{5}$$

where the coefficients are given by:

$$\begin{aligned} s_{10} &= \mu_0\alpha_1 + \mu_1\alpha_0, & d_{10} &= \mu_0\alpha_1 - \mu_1\alpha_0, \\ s_{21} &= \mu_2\alpha_1 + \mu_1\alpha_2, & d_{21} &= \mu_2\alpha_1 - \mu_1\alpha_2. \end{aligned} \tag{6}$$

Here, $\alpha_m = \sqrt{\lambda^2 + \gamma_m^2 + \omega^2\varepsilon_m\mu_m}$, and $\gamma_m = \sqrt{j\omega\mu_m(\sigma_m + j\omega\varepsilon_m)}$ is the propagation constant in medium

$m = 0, 1, 2$. The per-unit-length admittance matrix $\mathbf{Y}$ is related to the inverse of the potential matrix $\mathbf{P}$ as:

$$\mathbf{Y} = j\omega\,\mathbf{P}^{-1}. \tag{7}$$

The matrix $\mathbf{P}$ is defined as:

$$\mathbf{P} = (\mathbf{T}^{\mathsf{T}})^{-1}\left[\mathbf{U}\otimes\begin{bmatrix}P_{cs} & 0\\ 0 & P_{se}\end{bmatrix} + \mathbf{P}_e\otimes\begin{bmatrix}0 & 0\\ 0 & 1\end{bmatrix}\right]\mathbf{T}^{-1}, \tag{8}$$

where P_{cs} and P_{se} are the potential coefficients corresponding to the internal (core-to-sheath) and external (sheath-to-earth) insulation. The incidence matrix $\mathbf{T}$ is used to transform loop quantities to phase quantities:

$$\mathbf{T} = \mathbf{U}\otimes\begin{bmatrix}1 & 0\\ -1 & 1\end{bmatrix}. \tag{9}$$

The operator $(.)^t$ refers to the transpose of a matrix.

For cables buried in the upper soil layer, Papadopoulos et al. also proposed the following expression for the elements of the ground-return potential matrix:

$$P_{e,ij} = \frac{j\omega}{2\pi(\sigma_1 + j\omega\varepsilon_1)}\int_0^\infty [F(\lambda) + G(\lambda)]\cos(y_{ij}\lambda)\,d\lambda, \tag{10}$$

where

$$\begin{aligned} G(\lambda) &= 2\alpha_1\mu_1\mu_2(\gamma_1^2 - \gamma_2^2)(G_1(\lambda) + G_2(\lambda)) \\ &\quad +2\alpha_1\mu_0\mu_1(\gamma_1^2 - \gamma_0^2)(G_3(\lambda) + G_4(\lambda)). \end{aligned} \tag{11}$$

Expressions for $G_k(\lambda)$, with $k = 1, \ldots, 4$, are provided in Appendix A. The self-impedance and self-admittance corrections due to the earth can be obtained from (4) and (10), respectively, by setting y_{ij} to the cable outer radius and $h_j = h_i$. To decouple Equations (1a) and (1b), the product $\mathbf{YZ}$ is diagonalized via the modal transformation matrix $\mathbf{T}_I$, obtained by solving the eigenvalue problem:

$$\mathbf{T}_I^{-1}\mathbf{YZ}\mathbf{T}_I = \boldsymbol{\gamma}^2, \tag{12}$$

where $\boldsymbol{\gamma}^2 = \text{diag}(\gamma_1^2, \gamma_2^2, \ldots, \gamma_6^2)$, and γ_i are the modal propagation constants of the six modes.

Finally, for the three-phase SC cable system, the two-port nodal admittance equation can be formulated as:

$$\begin{bmatrix}\mathbf{I}(0)\\ \mathbf{0}\end{bmatrix} = \begin{bmatrix}\mathbf{A} & -\mathbf{B}\\ -\mathbf{B} & \mathbf{A} + \mathbf{Y}_L\end{bmatrix}\begin{bmatrix}\mathbf{V}(0)\\ \mathbf{V}(l)\end{bmatrix}, \tag{13}$$

where

$$\mathbf{A} = \mathbf{T}_I\,\text{diag}^{-1}(\tanh(\boldsymbol{\gamma}l))\,\text{diag}^{-1}(\boldsymbol{\gamma})\mathbf{T}_I^{-1}\mathbf{Y},$$

$$\mathbf{B} = \mathbf{T}_I\,\text{diag}^{-1}(\sinh(\boldsymbol{\gamma}l))\,\text{diag}^{-1}(\boldsymbol{\gamma})\mathbf{T}_I^{-1}\mathbf{Y}.$$

and

$$\begin{aligned} \mathbf{V} &= [V_{c1}, V_{s1}, V_{c2}, V_{s2}, V_{c3}, V_{s3}]^t \\ \mathbf{I} &= [I_{c1}, I_{s1}, I_{c2}, I_{s2}, I_{c3}, I_{s3}]^t \end{aligned}$$

with subscripts c and s referring to core and sheath, respectively. The cables are of length l and are connected to load admittances $\mathbf{Y}_s$ and $\mathbf{Y}_L$ at their input and output terminals.

3. SMITH AND LONGMIRE (LS) FREQUENCY-DEPENDENT SOIL MODEL

A realistic example of frequency-dependent soil is the model proposed by Longmire and Smith [15], commonly known as the **LS model**. It is a complex, broadband model suitable for representing permittivity and conductivity for different soil types, with empirical parameters obtained from experimental measurements. The model is valid in the frequency range from 100 Hz to 10^6 MHz [33]. In this work, Longmire and Smith model is used to investigate the frequency dependence of soil parameters on the transient response of the three-phase cable system buried in two-layer soil. According to [15], the frequency dependence relative permittivity ϵ_r and conductivity σ are given by:

$$\epsilon_r(f) = \epsilon_{r,\infty} + \sum_{n=1}^{13}\frac{a_n}{1 + \left(\frac{f}{f_n}\right)^2},\ \epsilon_r = \epsilon_{ri},\ i = 1, 2 \tag{14}$$

$$\sigma(f) = \sigma_{DC} + 2\pi f\epsilon_0\sum_{n=1}^{13}F_n\frac{a_n\left(\frac{f}{f_n}\right)^2}{1 + \left(\frac{f}{f_n}\right)^2},\ \sigma = \sigma_i \tag{15}$$

where σ_{DC} is the DC soil conductivity ($\sigma_{DC} = \sigma_{\text{DCi}},\ i = 1, 2$); $\epsilon_{r,\infty}$ is the high frequency limit of the relative permittivity ($\epsilon_{r,\infty} = 5$); and F_n is defined as:

$$F_n = (125\sigma_{DC})^{0.8312}\cdot 10^{n-1}\,[\text{Hz}] \tag{16}$$

and the coefficients a_n are given in Table 1.

TABLE 1. Coefficients for LS soil model.

n	a_n	n	a_n
1	$3.4\cdot 10^6$	8	$1.25\cdot 10^1$
2	$2.74\cdot 10^5$	9	$4.8\cdot 10^0$
3	$2.58\cdot 10^4$	10	$2.17\cdot 10^0$
4	$3.38\cdot 10^3$	11	$9.8\cdot 10^{-1}$
5	$5.26\cdot 10^2$	12	$3.92\cdot 10^{-1}$
6	$1.33\cdot 10^2$	13	$1.73\cdot 10^{-1}$
7	$2.72\cdot 10^1$		

Table 2 shows the electrical properties of the examined soils. In #$\mathbf{H}_1$ and #$\mathbf{H}_3$ cases, the soil is considered homogeneous with constant electrical parameters σ and $\epsilon_r = 5$ for the first case, and frequency-dependent $\sigma(f)$ and $\epsilon_r(f)$ according to the LS model for the second. In cases #$\mathbf{SFD}_1$ and #$\mathbf{SFD}_2$, the soil is stratified with two layers. The DC conductivities of the layers (LS model) are $\sigma_{1DC} = 0.01$ S/m and $\sigma_{2DC} = 0.001$ S/m for #$\mathbf{SFD}_1$. #$\mathbf{SFD}_2$ soil is characterized by $\sigma_{1DC} = 0.001$ S/m and $\sigma_{2DC} = 0.01$ S/m.

4. FIXING EIGENVALUE AND EIGENVECTOR SWITCHOVERS

By calculating the eigenvalues $\gamma_i^2,\ i = 1, \ldots, 6$ and associated eigenvectors $[\mathbf{T}_{I,*j},\ j = 1, \ldots, 6]$, where $\mathbf{T}_{I,*j}$ is the jth

TABLE 2. Examined soils properties.

Cases	Conductivity (S/m)
#$\mathbf{H}_1$	$\sigma = 0.01$
Homogeneous earth	$\sigma = 0.001$
#$\mathbf{H}_3$	$\sigma_{DC} = 0.01$
FD soil	$\sigma_{DC} = 0.001$
#$\mathbf{SFD}_1$	$\sigma_{1DC} = 0.01$
FD two-layer earth	$\sigma_{2DC} = 0.001$
#$\mathbf{SFD}_2$	$\sigma_{1DC} = 0.001$
FD two-layer earth	$\sigma_{2DC} = 0.01$

column-vector of the matrix $\mathbf{T}_I$ defined in (12), for each specific frequency using standard routines such as the Matlab eig(·) function, Mathematica Eigensystem[·] function using the direct method, QR algorithm, and power methods, the eigenvalues switching occurs. It also means that the relative positions of the columns $\mathbf{T}_{I,*j},\ j = 1, \ldots, 6$ change places at certain frequencies. This is because when the eigenproblem (12) is solved at a given frequency, conventional algorithms are unable to recover the relative order obtained at the previous frequency step, which makes them not suited for the evaluation of **YZ** eigenvectors as smooth frequency functions. In this work, **YZ** is calculated, and each element is divided by $-\omega^2\epsilon_0\mu_0$. The unit matrix **U** is subtracted, and the eigenvalues $\tilde{\gamma}_i^2$ and eigenvectors $\mathbf{T}_I$ of the modified matrix **S** [29]

$$\mathbf{S} = \frac{\mathbf{YZ}}{-\omega^2\epsilon_0\mu_0} - \mathbf{U} \tag{17}$$

are calculated. The real eigenvalues of **YZ** are then:

$$\gamma_i^2 = -\omega^2\epsilon_0\mu_0(1 + \tilde{\gamma}_i^2) \tag{18}$$

Figure 2 shows the frequency responses of the second column of the current modal transformation matrix $\mathbf{T}_I$ (real and imaginary parts) for horizontally arranged three-phase cables which are buried directly in the first layer of a frequency-dependent layered soil. The cables are located 1 m from the surface of the ground and are spaced 0.25 m apart. The first layer of # $\mathbf{SFD}_2$ soil is 3 m deep. The eigenvector matrix $\mathbf{T}_I$ is calculated from **S** matrix given in (18) using the MATHEMATICA Eigensystem[·] function.

As depicted in Figure 2(a), the components of the second eigenvector of **S** matrix exhibits discontinuities as the frequency changes, leading to switchovers in the propagation modes associated with the cable structure. The variation of the attenuation constants for the six modes ($\#i, i = 1, \ldots, 6$) of the cable system as a function of frequency is represented in Figure 3. As can be noticed in Figure 3(a), mode switching occurs at frequencies near 223.8 Hz, 274.15 Hz, and 1.71 MHz.

To ensure continuous and smooth **YZ** product eigenvectors over a wide range of frequencies, the proposed new method consists firstly in solving the modified eigenproblem

$$(\mathbf{S} - \tilde{\gamma}_k^2\mathbf{U})\mathbf{T}_{I,*k} = 0,\ k = 1, \ldots, 6 \tag{19}$$

$$\mathbf{T}_{I,*k} \cdot \mathbf{T}_{I,*k} = 1 \tag{20}$$

at the minimum frequency $f_{\min}$ of the set of frequency points $\{f_{\min}, f_{\min} + \triangle f, f_{\min}, +2\triangle f, \ldots, f_{\max}\}$ where $\triangle f$ is the frequency step using Mathematica Eigensystem[·]. The relationship (20) represents the normalization equation for the eigenvector $\mathbf{T}_{I,*k}$. The eigenvalues at $f_{\min}$ are denoted by $\bar{\gamma}_{1,1}^2, \bar{\gamma}_{1,2}^2, \ldots, \bar{\gamma}_{1,6}^2$, and their eigenvectors by $\bar{\mathbf{T}}_{I,*k}^1,\ k = 1, \ldots, 6$. After grouping (19) and (20), the complex-valued vector function **F** of size 7 is formulated and tends to zero for the pair of solutions **t** and λ, which respectively represent the 6×1-dimensional eigenvector of the **S** matrix and the corresponding eigenvalue

$$\mathbf{F}(\mathbf{X}) = \begin{pmatrix} \mathbf{S}\cdot\mathbf{t} - \lambda\mathbf{t} \\ \mathbf{t}\cdot\mathbf{t} - 1 \end{pmatrix} = \mathbf{0} \tag{21}$$

$$\mathbf{X} = (\mathbf{t}, \lambda)^t \tag{22}$$

The nonlinear system of Equation (21) can be solved by using several techniques [27, 28]. In this paper, an iteration procedure is proposed by applying a derivative-free iterative scheme which is based upon the divided difference operator (DDO) [29] as presented:

$$\begin{cases} \delta_n = [\zeta_n, \mathbf{X}_n; \mathbf{F}]^{-1} \cdot \mathbf{F}(\mathbf{X}_n) \\ \zeta_{n+1} = \mathbf{X}_n - \delta_n \\ \mathbf{Y}_n = \mathbf{X}_n + \delta_n \\ \mathbf{X}_{n+1} = \mathbf{Y}_n + [\zeta_{n+1}, \mathbf{X}_n; \mathbf{F}]^{-1} \cdot \mathbf{F}(\mathbf{Y}_n) \end{cases} \tag{23}$$

where $[\xi, \upsilon; \mathbf{F}]$ is the first order DDO of $\mathbf{F} = (F_1, F_2, \ldots, F_6)^t$ for the 6×1 dimensional nodes ξ and υ defined by a component-to-component procedure as follows:

$$[\xi, \upsilon; \mathbf{F}]_{i,j} = \frac{F_i(\xi_1, \ldots, \xi_j, \upsilon_{j+1}, \ldots, \upsilon_6)}{\xi_j - \upsilon_j} - \frac{F_i(\xi_1, \ldots, \xi_{j-1}, \upsilon_j, \ldots, \upsilon_6)}{\xi_j - \upsilon_j} \tag{24}$$

Next, each pair $(\bar{\mathbf{T}}_{I,*k}^1, \bar{\gamma}_{1,k}^2)^t$ is used as the initial guess $\mathbf{X}_1$ in the iterative process (23) to provide the correct eigenvalue-eigenvector pair $(\tilde{\mathbf{T}}_{I,*k}, \tilde{\gamma}_{1,k}^2)^t$ at frequency $f_{\min}$. The initial guess value ζ_1 is considered equal to $\mathbf{X}_1 + 0.0001\mathbf{Q}$ where $\mathbf{Q} = (1, \ldots, 1)^t$. The iteration stopping criteria, which correspond to both $|\mathbf{X}_{n+1} - \mathbf{X}_n|$ and $|\mathbf{F}(\mathbf{X_{n+1}})|$ less than a fixed tolerance ϵ, typically equal to 10^{-8}, are used. Finally, to ensure continuous, smooth behavior of the eigenvectors as a function of frequency and speed up the iteration process, the initial value of **X** at each frequency is seeded with the final solution at the previous frequency.

Figure 3(b) shows the attenuation constants obtained by applying the proposed method. It is obvious that there is no mode switching. Moreover, as depicted in Figure 2(b), the eigenvectors are continuous and smooth as a function of frequency. It should also be noted that the eigenvector switchover problem is altogether solved by the proposed method without the need for a sorting algorithm.

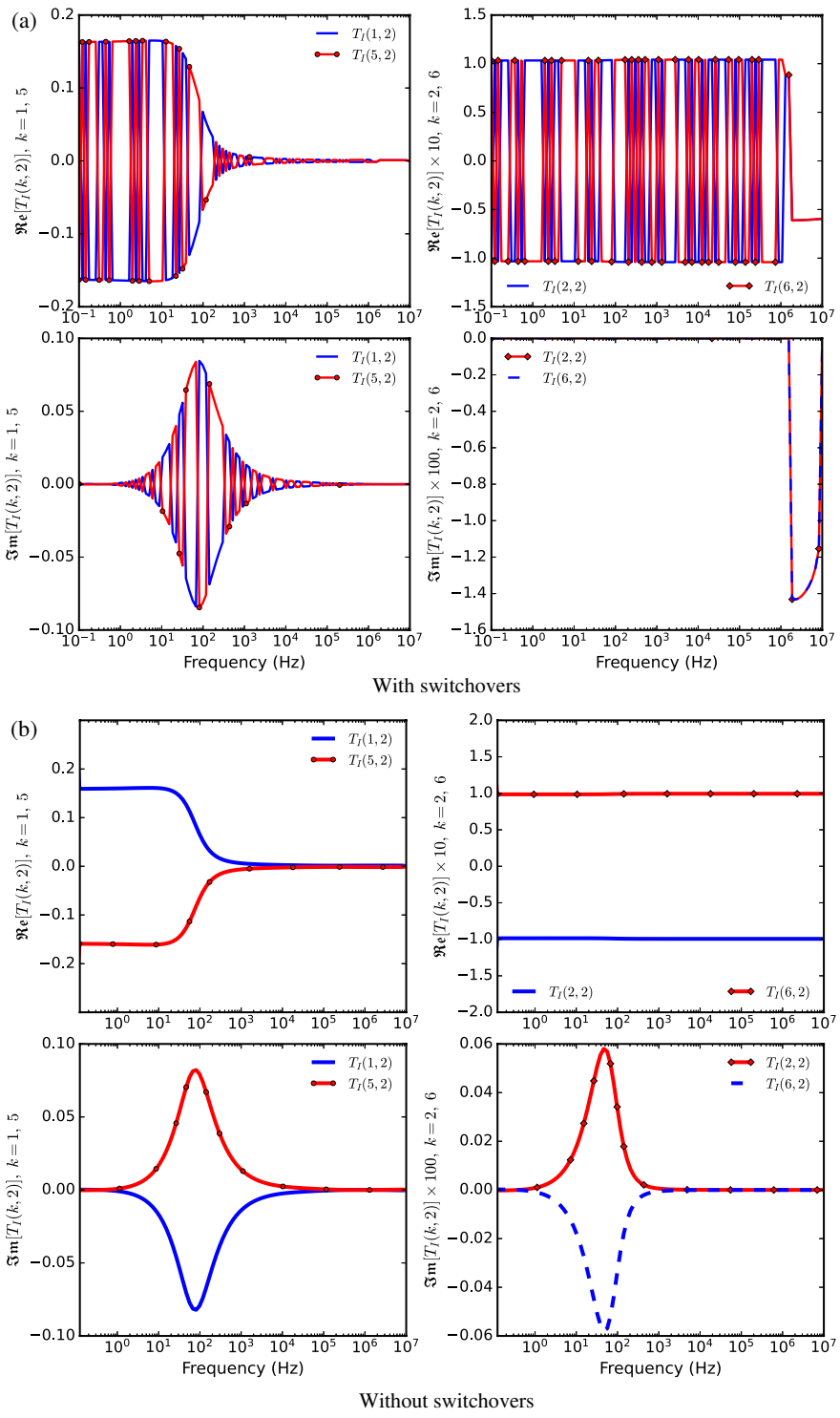

FIGURE 2. Magnitude of the real and imaginary elements of eigenvector 2 of **YZ** matrix.

5. TRANSIENT RESPONSES

To demonstrate the influence of soil stratification and frequency-dependent electrical properties on cable transient behavior, consider the three-phase horizontal SC cable system previously introduced in Figure 1. The cables, labeled C_1, C_2, and C_3, are identical. The soil specifications are listed in Table 2.

The transient responses are evaluated for various cable lengths and soil topologies. The soil may be homogeneous with constant (#$\mathbf{H}_1$) or frequency-dependent (#$\mathbf{H}_3$) parameters, or layered with frequency dependence, denoted as #$\mathbf{SFD}_1$ and #$\mathbf{SFD}_2$. The geometric layouts are shown in Figures 1 and 4.

A standard 1.2/50 µs lightning impulse voltage $v_i(t)$, of per-unit amplitude, is applied to the core of C_1 at the sending end, as illustrated in Figure 4. Cable sheaths are grounded through

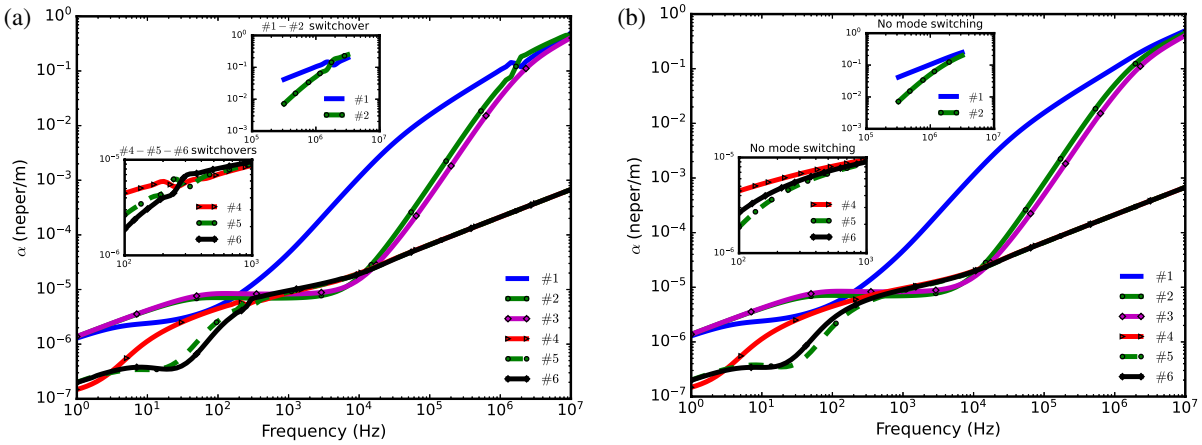

FIGURE 3. Comparison of modal attenuation constants for the cable system in #**SFD**$_2$ soil.

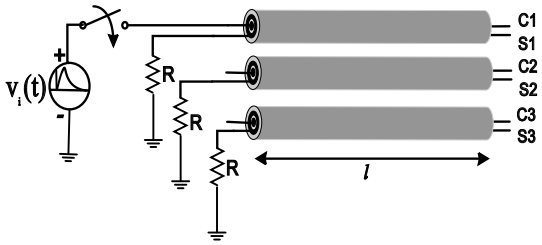

FIGURE 4. Test configuration for transient simulation.

a 1 Ω resistance. The nodal admittance matrix (13) is modified using Modified Nodal Analysis [30] to incorporate boundary conditions. Ground-return impedance expressions (4) and (10), involving semi-infinite integrals, are evaluated using the numerical integration method proposed in [31]. Time-domain responses are then recovered via Laplace Transform inversion using the Fast Fourier Transform in conjunction with the ε-algorithm to accelerate the convergence of the resulting infinite complex Fourier series [32].

Figure 5 summarizes the transient sheath voltage responses at the far end of cable C_1 in the MPS, under the four previously introduced soil topologies and three cable lengths ($l = 100$ m, 1000 m, and 4000 m). For each length, two conductivity values, 0.01 S/m and 0.001 S/m, are used to assess the influence of both soil stratification and FD electrical parameters.

For the short cable arrangement of length $l = 100$ m, the comparison between Figures 5(a) and 5(b) reveals a significant influence of soil conductivity. When the homogeneous soil conductivity is $\sigma = 0.01$ S/m, topology #$\mathbf{H}_1$ exhibits noticeable discrepancies compared to the frequency-dependent topology #$\mathbf{H}_3$ (with $\sigma_{DC} = 0.01$ S/m), as well as the stratified topology #$\mathbf{SFD}_1$ (with $\sigma_{1,DC} = 0.01$ S/m). These discrepancies, in peak amplitude and time delay, highlight the sensitivity of transient responses to both soil stratification and frequency dependence at higher conductivity.

At lower conductivity, these effects become even more pronounced: the amplitude of the transient sheath voltage is reduced by nearly half compared to the higher conductivity case, and the differences between topology #$\mathbf{H}_1$ (with $\sigma = 0.001$ S/m) and the frequency-dependent topologies (with $\sigma_{DC} = \sigma_{1,DC} = 0.001$ S/m) become more distinct. It indicates the dominant role of frequency-dependent parameters in strongly influencing the transient response in low-conductivity environments.

For a cable length of $l = 1000$ m, Figures 5(c) and 5(d) show a decreasing sensitivity to both soil stratification and frequency dependence electrical parameters. Under higher conductivity conditions, the transient responses for topologies #$\mathbf{H}_1$, #$\mathbf{H}_3$, and #$\mathbf{SFD}_1$ become nearly indistinguishable, indicating that the influence of frequency-dependence and stratification diminishes at this length.

At lower conductivity, minor variations persist between the homogeneous and frequency-dependent topologies; however, the overall trend remains: the impact of soil electrical properties on transient voltages becomes less pronounced as the cable length increases.

For the longest cable arrangement, with a length of $l = 4000$ m, Figures 5(e) and 5(f) confirm this trend. The transient sheath voltage responses for the three configurations, #$\mathbf{H}_1$, #$\mathbf{H}_3$, and #$\mathbf{SFD}_1$, with $\sigma = \sigma_{DC} = \sigma_{1,DC}$ are nearly identical for both conductivity values. Additionally, the deviation previously observed in topology #$\mathbf{SFD}_2$ becomes significantly reduced, reinforcing the conclusion that the impact of soil characteristics on transient behavior weakens with increasing cable length.

These observations collectively suggest that, while frequency dependence and stratification have a considerable impact at short lengths and low conductivities, their influence becomes progressively negligible as the cable length increases.

Figure 6 illustrates both the primary and the equivalent MPS models employed in the transient simulations. In the primary MPS configuration, three identical cables, each with a length of $l = 1$ km, are positioned at distinct vertical locations.

Cables C_1 and C_3 are located at a depth of $h_{1,3} = 2$ m below ground level, whereas the middle cable, C_2, is situated at $h_2 = 1$ m, all embedded within the first soil layer of thickness $d = 3$ m in a frequency-dependent stratified medium. A

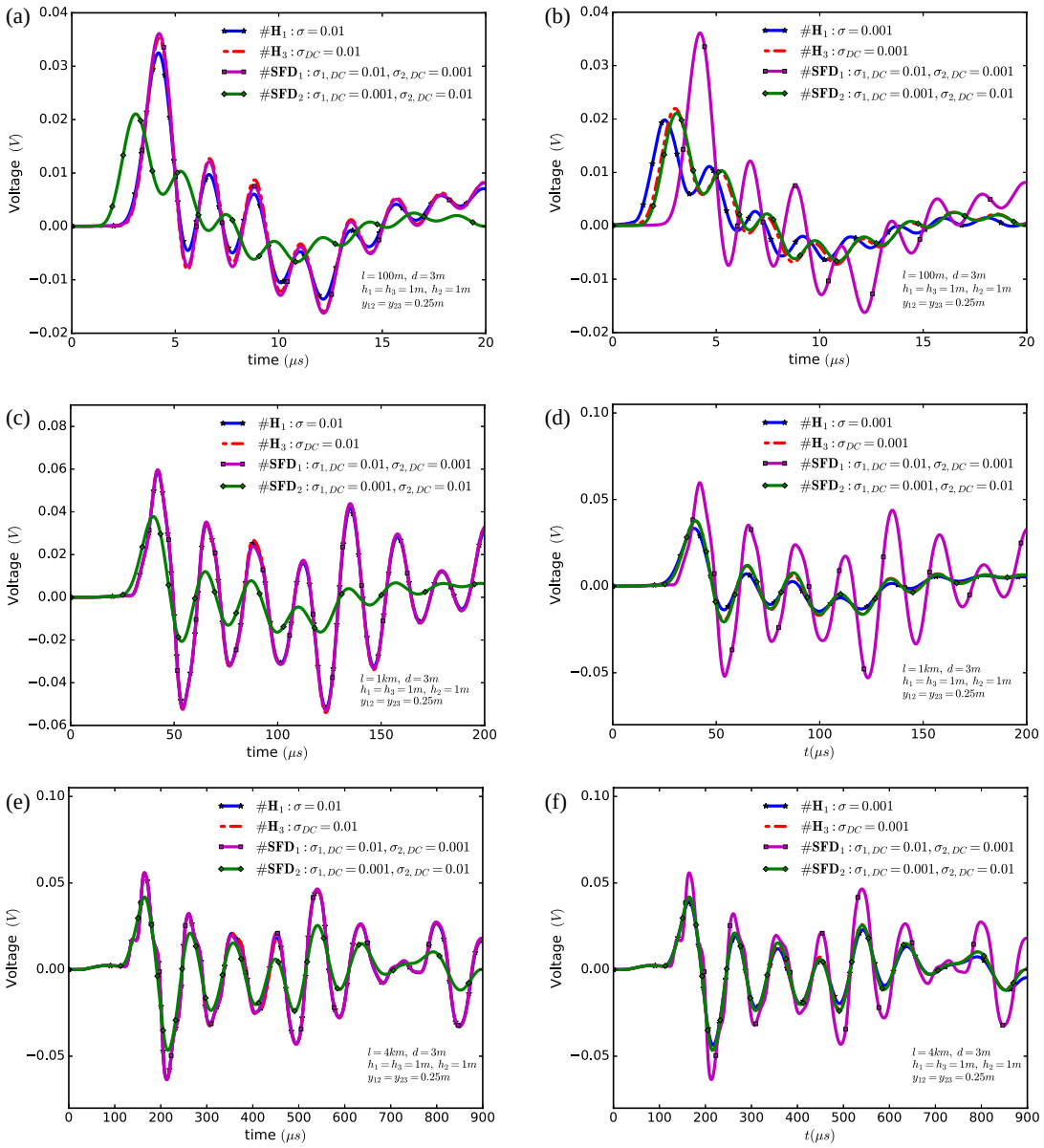

FIGURE 5. Comparison of transient sheath voltage responses at the far end of the first cable for two conductivities: 0.01 and 0.001 S/m.

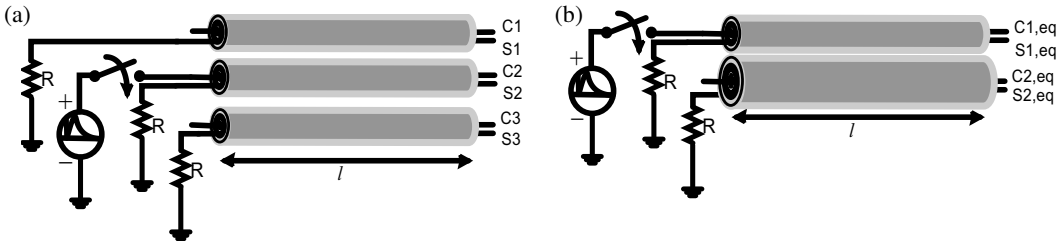

Three-conductor configuration Equivalent two-conductor configuration

FIGURE 6. Primary and equivalent MPS configurations employed for transient analysis.

double-exponential voltage source is applied exclusively to the core of the central cable C_2.

In the equivalent two-conductor model, cables C_1 and C_3 are replaced by a single equivalent cable denoted as $C_{2,\text{eq}}$, while the central cable C_2 is represented by $C_{1,\text{eq}}$. In this configuration, the excitation is applied to the core of $C_{1,\text{eq}}$.

The geometric layout of the equivalent MPS model, comprising cables $C_{1,\text{eq}}$ with radius r_1 and $C_{2,\text{eq}}$ and radius $r_{\text{eq}} = r_4|y_1 - y_3|$, is shown in Figure 7.

These conductors are embedded in a two-layer soil characterized by DC conductivities $\sigma_{1,DC}$ and $\sigma_{2,DC}$.

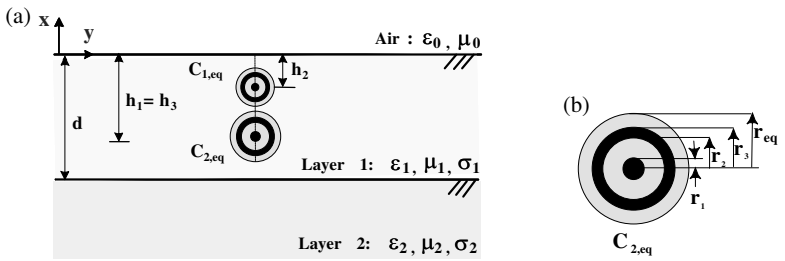

Geometric configuration of equivalent SC cables

Equivalent underground cable cross-section

FIGURE 7. Geometric configuration in two-layer soil of the equivalent MPS.

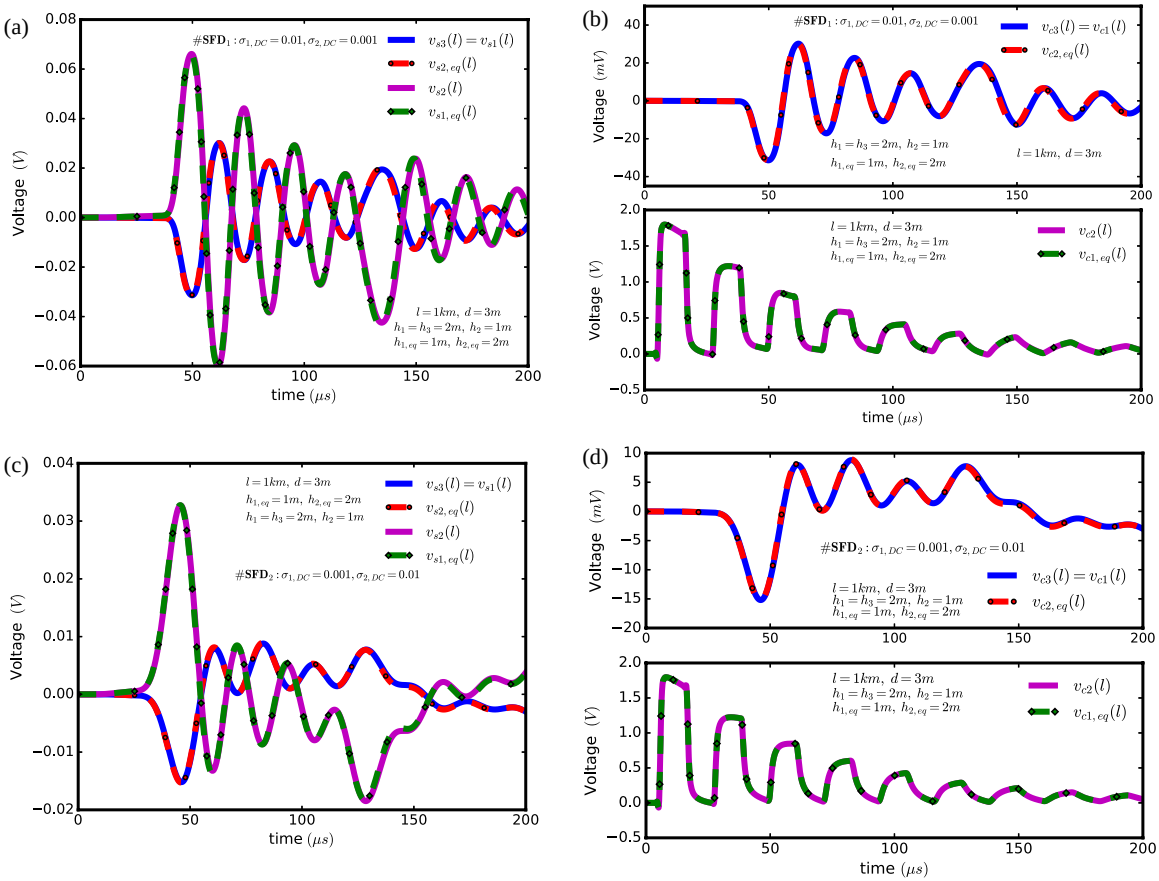

FIGURE 8. Transient core and sheath voltage responses for two FD conductivity configurations: (**SFD**$_1$) and (**SFD**$_2$).

Figure 8 compares the transient voltages at the cores and sheaths of the cables for both the primary and equivalent models. In the equivalent configuration, the first equivalent cable $C_{1,\text{eq}}$ is excited, analogous to the excitation of cable C_2 in the primary MPS configuration. The results presented in Figures 8(a) and 8(c) demonstrate that the sheath voltages of cable C_2 can be accurately estimated using the equivalent two-phase model. Similarly, the voltages in cables C_1 and C_3, which are electrically identical, are well reproduced by the equivalent cable $C_{2,\text{eq}}$ for both soil topologies #**SFD**$_1$ and #**SFD**$_2$. This equivalence remains valid provided that the cables sharing identical electrical characteristics, are subjected to the same excitation, and are terminated with identical load impedances.

A similar observation applies to the core voltages of cables C_1 and C_3, which closely match the transient voltage at the core of the equivalent cable $C_{2,\text{eq}}$, as shown in Figures 8(b) and 8(d). A noticeable reduction in the amplitude of the core voltage of $C_{2,\text{eq}}$ is observed as a consequence of changes in soil topology.

A noteworthy finding is that the transient voltage response at the core remains identical for both soil configurations #**SFD**$_1$ and #**SFD**$_2$. This consistency is attributed to the dominant influence of the impulse voltage source, which is largely unaffected by variations in soil electrical parameters.

It should be noted that the sheath transient voltages at the receiving end of cable C1 for soil topology #**H**$_3$ and cable lengths $l = 100$ m, $l = 1$ km, and $l = 4$ km in the flat three-phase configuration are exactly those obtained in [34] (see Figures 10(a), (c), and (e), reported in [34], for a generalized approach and a flat configuration). This agreement in results validates the proposed methods for eliminating mode switching, calculating the

generalized earth return impedance and admittance for buried cables, and evaluating transient voltages in underground MPS.

6. CONCLUSION

In this paper, the influence of soil stratification and the frequency dependence of electrical parameters on the transient behavior of underground cables in a multi-phase system configuration has been investigated.

An improved method was first proposed to compute smooth modal transformation matrices in the frequency domain using a derivative-free iterative approach. This robust technique addresses the challenging switchover eigenproblem and provides a reliable foundation for accurately modeling the modal behavior of underground MPS configurations.

The impact of soil stratification and frequency-dependent electrical parameters on the transient responses of MPS cables was thoroughly examined using Modified Nodal Analysis. The results show that, while these factors, especially soil conductivity (i.e., FD conductivity), strongly influence the transient behavior of short cables, their effect significantly diminishes with increasing cable length. For longer cables, transient voltages become less sensitive to soil stratification, provided that the conductivity of the surrounding burial medium remains constant. This observation suggests that simplified homogeneous soil models may be sufficiently accurate for long-distance simulations.

Furthermore, this study validates an equivalent cable reduction technique for MPS configurations, in which two identical, symmetrically placed cables are replaced by a single equivalent conductor with an appropriate radius. This method accurately preserves both core and sheath voltage responses, as confirmed by the strong agreement between the full and reduced models. The proposed approach thus offers a robust and computationally efficient alternative for simulating transients in underground cables embedded in complex soil environments.

APPENDIX A.

The terms $G_i(\lambda)$ appearing in expression (11) for the function $G(\lambda)$ are defined as:

$$\boldsymbol{G}_1(\lambda) = \frac{S_{10}A_{10}e^{-\alpha_1(2d-h_1-h_2)} - D_{10}\Lambda_{21}e^{-\alpha_1(2d+h_1-h_2)}}{(A_{10}A_{21}+\Delta_{10}\Delta_{21}e^{-2\alpha_1 d})(S_{10}S_{21}+D_{10}D_{21}e^{-2\alpha_1 d})}$$

$$\boldsymbol{G}_2(\lambda) = \frac{S_{10}\Delta_{10}e^{-\alpha_1(2d-h_1+h_2)} - D_{10}\Delta_{10}e^{-\alpha_1(2d+h_1+h_2)}}{(A_{10}A_{21}+\Delta_{10}\Delta_{21}e^{-2\alpha_1 d})(S_{10}S_{21}+D_{10}D_{21}e^{-2\alpha_1 d})}$$

$$\boldsymbol{G}_3(\lambda) = \frac{S_{21}\Delta_{12}e^{-\alpha_1(2d+h_1-h_2)} + D_{21}\Delta_{21}e^{-\alpha_1(2d+h_1+h_2)}}{(A_{10}A_{21}+\Delta_{10}\Delta_{21}e^{-2\alpha_1 d})(S_{10}S_{21}+D_{10}D_{21}e^{-2\alpha_1 d})}$$

$$\boldsymbol{G}_4(\lambda) = \frac{S_{21}\Delta_{12}e^{-\alpha_1(h_1+h_2)} + D_{21}\Delta_{21}e^{-\alpha_1(2d-h_1+h_2)}}{(A_{10}A_{21}+\Delta_{10}\Delta_{21}e^{-2\alpha_1 d})(S_{10}S_{21}+D_{10}D_{21}e^{-2\alpha_1 d})}$$

Assuming the indices $\{p, n = 0, 1, 2\}$, the auxiliary terms are defined as:

$$S_{pn} = \mu_n\alpha_p + \mu_p\alpha_n, \quad A_{pn} = \alpha_n\gamma_p^2\mu_n + \alpha_p\gamma_n^2\mu_p$$

$$D_{pn} = \mu_n\alpha_p + \mu_p\alpha_n, \quad \Delta_{pn} = \alpha_n\gamma_p^2\mu_n - \alpha_p\gamma_n^2\mu_p$$

REFERENCES

[1] Pollaczek, F., "Uber das Feld einer unendlich langen wechselstromdurch-flossen Einfachleitung," *Elektr. Nachr. Technik*, Vol. 3, No. 9, 339–360, 1926.

[2] Sunde, E. D., *Earth Conduction Effects in Transmission Systems*, 2nd ed., 99–139, Dover Publications, New York, NY, USA, 1968.

[3] Carson, J. R., "Ground return impedance: Underground wire with earth return," *Bell System Technical Journal*, Vol. 8, No. 1, 94–98, 1929.

[4] Wait, J. R., "Electromagnetic wave propagation along a buried insulated wire," *Canadian Journal of Physics*, Vol. 50, No. 20, 2402–2409, 1972.

[5] Bridges, G. E. J., "Fields generated by bare and insulated cables buried in a lossy half-space," *IEEE Transactions on Geoscience and Remote Sensing*, Vol. 30, No. 1, 140–146, Jan. 1992.

[6] Zhang, B., J. Zou, X. Du, J. Lee, and M.-N. Ju, "Ground admittance of an underground insulated conductor and its characteristic in lightning induced disturbance problems," *IEEE Transactions on Electromagnetic Compatibility*, Vol. 59, No. 3, 894–901, Jun. 2017.

[7] Papadopoulos, T. A., D. A. Tsiamitros, and G. K. Papagiannis, "Impedances and admittances of underground cables for the homogeneous earth case," *IEEE Transactions on Power Delivery*, Vol. 25, No. 2, 961–969, Apr. 2010.

[8] Xue, H., A. Ametani, J. Mahseredjian, and I. Kocar, "Generalized formulation of earth-return impedance/admittance and surge analysis on underground cables," *IEEE Transactions on Power Delivery*, Vol. 33, No. 6, 2654–2663, Dec. 2018.

[9] Li, Z., J. He, B. Zhang, and Z. Yu, "Influence of frequency characteristics of soil parameters on ground-return transmission line parameters," *Electric Power Systems Research*, Vol. 139, 127–132, 2016.

[10] De Conti, A. and M. P. S. Emidio, "Extension of a modal-domain transmission line model to include frequency-dependent ground parameters," *Electric Power Systems Research*, Vol. 138, 120–130, 2016.

[11] De Lima, A. C. S. and C. Portela, "Inclusion of frequency-dependent soil parameters in transmission-line modeling," *IEEE Transactions on Power Delivery*, Vol. 22, No. 1, 492–499, Jan. 2007.

[12] Garbelim Pascoalato, T. F., A. R. J. de Araújo, J. S. L. Colqui, S. Kurokawa, and J. P. Filho, "A comparison of frequency-dependent soil models: Electromagnetic transient analysis of overhead transmission lines using modal decomposition," *Energies*, Vol. 15, No. 5, 1687, 2022.

[13] Papadopoulos, T. A., Z. G. Datsios, A. I. Chrysochos, P. N. Mikropoulos, and G. K. Papagiannis, "Impact of the frequency-dependent soil electrical properties on the electromagnetic field propagation in underground cables," in *International Conference*

on Power Systems Transients (IPST), Perpignan, France, Jun. 2019.

[14] Xue, H., A. Ametani, Y. Liu, and J. D. Silva, "Effect of frequency-dependent soil parameters on wave propagation and transient behaviors of underground cables," *International Journal of Electrical Power & Energy Systems*, Vol. 122, 106163, 2020.

[15] Longmire, C. L. and K. S. Smith, "A universal impedance for soils," Topical Report, Defense Nuclear Agency, Santa Barbara, CA, USA, 1975.

[16] Alipio, R. and S. Visacro, "Modeling the frequency dependence of electrical parameters of soil," *IEEE Transactions on Electromagnetic Compatibility*, Vol. 56, No. 5, 1163–1171, Oct. 2014.

[17] Datsios, Z. and P. N. Mikropoulos, "Characterization of the frequency dependence of the electrical properties of sandy soil with variable grain size and water content," *IEEE Transactions on Dielectrics and Electrical Insulation*, Vol. 26, No. 3, 904–912, Jun. 2019.

[18] Marti, L., "Simulation of transients in underground cables with frequency-dependent modal transformation matrices," *IEEE Transactions on Power Delivery*, Vol. 3, No. 3, 1099–1110, Jul. 1988.

[19] Carson, J. R., "Wave propagation in overhead wires with ground return," *The Bell System Technical Journal*, Vol. 5, No. 4, 539–554, 1926.

[20] Nakagawa, M. and K. Iwamoto, "Earth-return impedance for the multi-layer case," *IEEE Transactions on Power Apparatus and Systems*, Vol. 95, No. 2, 671–676, Mar. 1976.

[21] Papadopoulos, T. A., Z. G. Datsios, A. I. Chrysochos, P. N. Mikropoulos, and G. K. Papagiannis, "Wave propagation characteristics and electromagnetic transient analysis of underground cable systems considering frequency-dependent soil properties," *IEEE Transactions on Electromagnetic Compatibility*, Vol. 63, No. 1, 259–267, 2021.

[22] Papadopoulos, T. A., D. A. Tsiamitros, and G. K. Papagiannis, "Earth return admittances and impedances of underground cables in non-homogeneous earth," *IET Generation, Transmission & Distribution*, Vol. 5, No. 2, 161–171, 2011.

[23] Ametani, A., T. Ohno, and N. Nagaoka, *Cable System Transients: Theory, Modeling and Simulation*, 1st ed., Wiley-IEEE Press, 2015.

[24] Paul, C. R., *Analysis of Multiconductor Transmission Lines*, 2nd ed., Wiley-IEEE Press, 2007.

[25] Zlatunić, I., S. Vodopija, and R. Goić, "Mode switching in modal domain models of overhead lines and underground cables," in *IPST — International Conference on Power System Transients, Paper*, No. 15IPST203, 2015.

[26] Wedepohl, L. M., H. V. Nguyen, and G. D. Irwin, "Frequency-dependent transformation matrices for untransposed transmission lines using Newton-Raphson method," *IEEE Transactions on Power Systems*, Vol. 11, No. 3, 1538–1546, Aug. 1996.

[27] Chrysochos, A. I., T. A. Papadopoulos, and G. K. Papagiannis, "Robust calculation of frequency-dependent transmission-line transformation matrices using the Levenberg-Marquardt method," *IEEE Transactions on Power Delivery*, Vol. 29, No. 4, 1621–1629, Aug. 2014.

[28] Galloway, R. H., W. B. Shorrocks, and L. M. Wedepohl, "Calculation of electrical parameters for short and long polyphase transmission lines," in *Proceedings of the Institution of Electrical Engineers*, Vol. 111, No. 12, 2051–2059, 1964.

[29] Rostami, M., T. Lotfi, and A. Brahmand, "A fast derivative-free iteration scheme for nonlinear systems and integral equations," *Mathematics*, Vol. 7, No. 7, 637, 2019.

[30] Griffith, J. R. and M. S. Nakhla, "Time-domain analysis of lossy coupled transmission lines," *IEEE Transactions on Microwave Theory and Techniques*, Vol. 38, No. 10, 1480–1487, Oct. 1990.

[31] Belganche, Z., A. Maaouni, A. Mzerd, and A. Bouziane, "Equivalent model from two layers stratified media to homogeneous media for overhead lines," *Progress In Electromagnetics Research M*, Vol. 41, 63–72, 2015.

[32] Brancik, L., "Programs for fast numerical inversion of Laplace transforms in MATLAB language environment," in *Proceedings of the 7th Conference MATLAB*, Vol. 99, 27–39, 1999.

[33] Cavka, D., N. Mora, and F. Rachidi, "A comparison of frequency-dependent soil models: Application to the analysis of grounding systems," *IEEE Transactions on Electromagnetic Compatibility*, Vol. 56, No. 1, 177–187, Feb. 2014.

[34] Papadopoulos, T. A., Z. G. Datsios, A. I. Chrysochos, P. N. Mikropoulos, and G. K. Papagiannis, "Modal propagation characteristics and transient analysis of multiconductor cable systems buried in lossy dispersive soils," *Electric Power Systems Research*, Vol. 196, 107249, 2021.